

Elastic Instabilities of Polymer Solutions in Cross-Channel Flow

P. E. Arratia,^{1,2} C. C. Thomas,¹ J. Diorio,¹ and J. P. Gollub^{1,2}

¹Physics Department, Haverford College, Haverford, Pennsylvania 19041, USA

²Physics Department, University of Pennsylvania, Philadelphia, Pennsylvania 19104, USA

(Received 13 September 2005; published 14 April 2006)

When polymer molecules pass near the hyperbolic point of a microchannel cross flow, they are strongly stretched. As the strain rate is varied at low Reynolds number ($< 10^{-2}$), tracer and particle-tracking experiments show that molecular stretching produces two flow instabilities: one in which the velocity field becomes strongly asymmetric, and a second in which it fluctuates nonperiodically in time. The flow is strongly perturbed even far from the region of instability, and this phenomenon can be used to produce mixing.

DOI: [10.1103/PhysRevLett.96.144502](https://doi.org/10.1103/PhysRevLett.96.144502)

PACS numbers: 47.50.-d, 05.45.-a, 83.50.-v, 83.60.Wc

The rheology of polymeric fluids is often complex, and their material properties have a strong impact on flow behavior. It has long been observed that the presence of polymer molecules in a fluid can lead to flow instabilities and nonlinear dynamics [1–7]. For example, Giesekus [3] observed a cellular instability of a non-Newtonian fluid in Taylor-Couette flows, analogous to the classical Taylor-Couette instability of Newtonian fluids, but at very low Reynolds (Taylor) numbers. Later, Larson, Shaqfeh, and Muller [8] demonstrated that these non-Newtonian instabilities are caused by fluid elasticity. Groisman and Steinberg [9] demonstrated an increased flow resistance and statistical properties typical of turbulence in polymeric fluids at very low Reynolds numbers. They found that viscoelasticity can enhance mixing in small curved channels [10].

Macroscopic non-Newtonian behavior results from microscopic stresses due to flow-induced changes in polymer conformation in solution. These stresses depend on the nature of the flow. For example, it has been shown that elongational (or extensional) flows can stretch and orient polymer molecules to a greater extent than ordinary shear flows [11]. The behavior of polymer solutions in extensional flow has received growing attention [12–15]. Theoretical investigations [16,17] predict that a flexible polymer molecule that is initially coiled at rest can be fully stretched if subjected to uniaxial extensional flow at sufficiently high strain rates. This is the so-called “coil-stretch” transition, which is predicted to occur at $\dot{\epsilon} \approx 0.5\lambda^{-1}$ [18], where λ is the relaxation time of the fluid and $\dot{\epsilon}$ is the strain rate. Early experiments in a cross-channel geometry using birefringence showed that molecules are extended in large strain fields, and that they align with the flow [19–22]. Later experiments capable of imaging individual polymer molecules (DNA) near the stagnation point in a cross-channel flow [12,23] found evidence of a sharp hysteretic transition from the coiled to the stretched state [24]. At high strain rates, distinct molecular conformations with different dynamics were observed. An important question is how polymer molecules that are

driven away from equilibrium affect the bulk flow behavior in a simple extensional flow.

In this Letter, we report two novel flow instabilities of a planar extensional flow of a dilute flexible polymer solution under steady forcing. In the first instability, the flow becomes deformed and asymmetric but remains steady. In a further instability that occurs at higher strain rates, the velocity field fluctuates nonperiodically in time and can produce mixing. Viscous Newtonian fluids, and a dilute semirigid polymer solution, are devoid of instabilities under these conditions (low Reynolds number).

An extensional flow is generated in a flow cell consisting of crossed channels that are $650 \mu\text{m}$ wide and $500 \mu\text{m}$ deep [Fig. 1(a)]. Because of the small length scale ($L = 650 \mu\text{m}$) the Reynolds number (Re) is small ($\text{Re} < 10^{-2}$). Here, $\text{Re} = LU\rho/\eta$, where U is the rms velocity, ρ is the fluid density, and η is the fluid viscosity. For the polymeric fluid, we also define the Deborah number (De), which is the product of the longest relaxation time of the fluid (λ) and the flow strain rate ($\dot{\epsilon}$). The polymer used here is high molecular weight polyacrylamide (PAA, 18×10^6 MW), which has a flexible backbone. The flexible polymeric solution is made by adding 200 ppm of PAA to a viscous Newtonian solvent (97%-glycerol aqueous solution). The solution is considered dilute; the overlap concentration (c^*) for PAA solutions is approximately 350 ppm ($c/c^* = 0.57$). The fluid is characterized using a stress-controlled rheometer at 25°C . The shear viscosity η of the PAA solution is nearly constant at 1.18 Pa s, for strain rates up to 10 s^{-1} . This behavior is typical of Boger fluids [25]. The longest relaxation time (λ) is obtained using a direct measurement of the first normal stress difference (N_1), which is nearly proportional to the mean square shear rate $\dot{\gamma}^2$ at low shear rates. Using the Oldroyd-B rheological model, which is generally thought to be appropriate for these solutions, $\lambda = \Psi_1/2(\eta - \eta_s)$ [26], where the first normal stress coefficient is $\Psi_1 = N_1/\dot{\gamma}^2 \approx 9.44 \text{ Pa s}^2$ in the limit of low shear rate. Here, η_s refers to the solvent viscosity. We find that $\lambda = 12.4(\pm 0.4) \text{ s}$. However, other models would yield different relaxation times, and there-

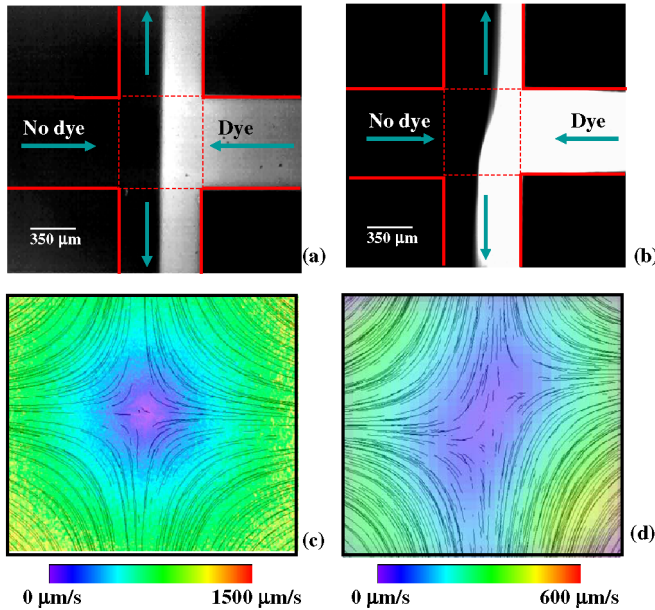


FIG. 1 (color online). Dye advection patterns for a cross-channel flow with two inputs and two outputs at low $Re (< 10^{-2})$ for (a) Newtonian fluid, and (b) PAA flexible polymer solution (strain rate $\dot{\epsilon} = 0.36 \text{ s}^{-1}$, Deborah number $De = 4.5$), where the interface between dyed and undyed fluid is deformed by an instability. (c),(d) Particle streak lines and velocity field magnitudes corresponding to (a),(b), showing the symmetry-breaking instability.

fore different values of De than those quoted here. Therefore, in presenting our results, we also quote the 2D strain rate $\dot{\epsilon}$.

Fluorescein dye at concentration $1 \times 10^{-3} \text{ M}$ can be added for visualization. Fluid is injected into the cross-slot geometry using syringe pumps; the flow rate is constant to about 1.0% at each flow rate. We also measure velocity fields by tracking small fluorescent particles ($5 \mu\text{m}$ diameter) seeded in the fluid.

To demonstrate the first instability, we show the results of dye advection experiments using an epifluorescence microscope in which a blue light illuminates the cross-slot region, where the flow is strongly extensional. (There is also, of course, some vorticity due to the upper and lower boundaries of the flow channel.) A small quantity of dyed solution (bright) is injected into one inlet, while undyed polymer solution (dark) is injected into the other inlet. Figure 1(a) shows the results for a Newtonian fluid (99% glycerol, $\eta = 0.8 \text{ Pa s}$) at $Re = 7 \times 10^{-3}$. The snapshot reveals a sharp interface at the center of the cross-slot region between the dye and undyed fluids, which demonstrates that this fluid does not mix.

Figure 1(b) reveals an entirely different behavior if we replace the Newtonian fluid by the dilute PAA solution ($\eta = 1.18 \text{ Pa s}$), for a strain rate estimated from the measured 2D velocity field near the center height of the channel to be $\dot{\epsilon} = 0.36 \text{ s}^{-1}$, or $De = 4.5$. (Velocity gradients

perpendicular to the plane of the channel are small near the center plane.) The snapshot of the advected dye pattern shows that the interface is deformed (wavy), although still sharp. The pattern is steady and does not change significantly over several minutes. The mirror image of this pattern can also occur, depending on initial conditions. That is, the flow is bistable [27,28].

Figure 1(c) shows both typical particle paths and the magnitude of the time-independent velocity field of the Newtonian fluid in the cross-slot region: a well-defined symmetric extensional flow. Note that the velocity vanishes at the stagnation point at the center of the cross-slot, where the strain rate is highest, and the fluid is most strongly stretched. The velocity field [Fig. 1(d)] shows a deformed and asymmetric flow for the PAA solution.

The flow field for the PAA solution becomes time dependent when $\dot{\epsilon} > 1 \text{ s}^{-1}$ ($De > 12.5$). We illustrate this time dependence by showing a series of dye advection images Figs. 2(a)–2(c) at $\dot{\epsilon} = 2.13 \text{ s}^{-1}$ ($De = 26.4$). These are consecutive snapshots of dye fields in the cross slot, taken 1.75 s apart. The dye pattern oscillates, as can be illustrated by following the interface between the dyed and undyed fluids. At a given instant, the dyed solution no longer divides equally between the two outlets. The interface between the fluids is not as sharp as before [e.g., Fig. 1(c)]. This indicates that the three-dimensional structure is more complex than in the steady case.

To quantify the time dependence of the flow, we sample a small square region in the cross slot (about 23% of the

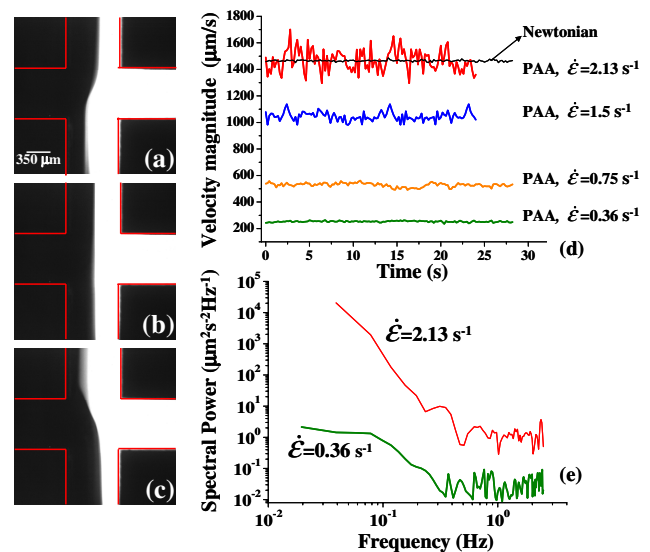


FIG. 2 (color online). (a)–(c) Dye advection patterns for the PAA solution in the time-dependent regime ($\dot{\epsilon} = 2.13 \text{ s}^{-1}$, $De = 26.4$) at 1.75 s intervals. (d) Velocity magnitude, averaged over the central 23% of the intersection region, for PAA at various $\dot{\epsilon}$ and (in one case) for the Newtonian fluid. The flexible polymer solution becomes time dependent for sufficiently large $\dot{\epsilon}$. (e) Corresponding power spectra of the velocity measurements for $\dot{\epsilon} = 0.36 \text{ s}^{-1}$ and $\dot{\epsilon} = 2.13 \text{ s}^{-1}$.

channel width, centered on the stagnation point), and measure the average speed in that region as a function of time. Sampling times are long enough to ensure the accuracy of the velocimetry measurement (10 ms), but are much shorter than the typical time scale of the fluid motion (of order 2 s). Sequences of velocity records for flow at several strain rates for PAA solutions, and for a Newtonian case, are shown in Fig. 2(d). As $\dot{\epsilon}$ is increased, the speed fluctuations become larger. The Newtonian case produces no such fluctuations at comparable strain rates.

The corresponding power spectra of the local speed (velocity magnitude) are shown for two values of $\dot{\epsilon}$ in Fig. 2(e). Since the entire velocity field must be measured at each instant, the records are only a few hundred points long, but this is sufficient to establish the qualitative features of the spectra. The spectral power at low frequencies grows by 2–4 orders of magnitude as $\dot{\epsilon}$ is increased from 0.36 to 2.13 s⁻¹. The speed fluctuations (and also the fluctuations of the individual velocity components) are nonperiodic, with a possible power-law spectral decay. The corresponding spectrum for the Newtonian case is nearly flat. Power-law spectra for sheared polymer solutions at low Re have been demonstrated [9], but the extensional case has not been previously reported. Despite temporal fluctuations in the velocity field, no mixing is observed in the cross-slot region.

Next, we examine the variation of the velocity field with $\dot{\epsilon}$ and De in Fig. 3. At low $\dot{\epsilon}$ ($\dot{\epsilon} = 0.1$ s⁻¹, De = 1.2) the velocity field resembles the Newtonian case in that it is symmetric and steady [Fig. 3(a)]. The developing asymmetry is evident at $\dot{\epsilon} = 0.36$ s⁻¹ (De = 4.5), but the flow

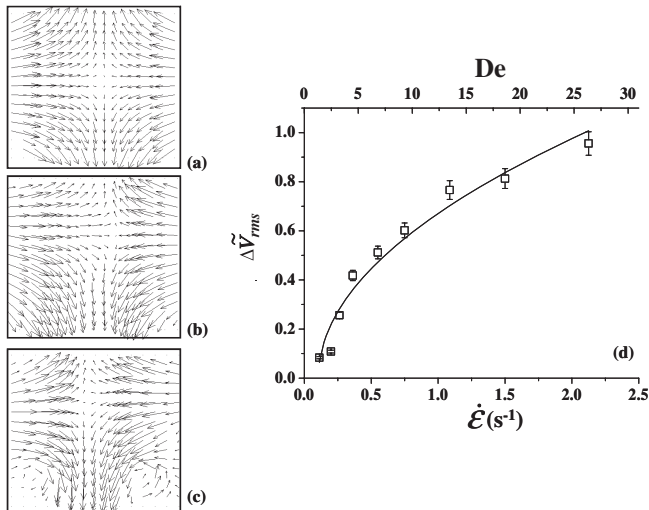


FIG. 3. Velocity fields at (a) $\dot{\epsilon} = 0.1$ s⁻¹ (De = 1.2, steady), (b) $\dot{\epsilon} = 0.36$ s⁻¹ (De = 4.5, steady and asymmetric), and (c) $\dot{\epsilon} = 2.13$ s⁻¹ (De = 26.4, time dependent and asymmetric). The region shown is 600×600 μm . (d) Normalized rms deviation $\Delta \tilde{V}_{rms}$ of PAA velocity fields from the Newtonian case at the same shear rate (see text), along with a fit to the expected square root law for a normal bifurcation.

remains steady [Fig. 3(b)]. As $\dot{\epsilon}$ is further increased to 2.13 s⁻¹ (De = 26.4), we note the appearance of vortices, as shown in Fig. 3(c). These vortices fluctuate in space and time, rendering the velocity field time dependent. We estimate the onset of time dependence to occur approximately at $\dot{\epsilon} = 1.0$ s⁻¹ (De = 12.5). Flow asymmetry and time-dependent velocity fields have also been reported in macroscopic entry (contraction) flows at higher Re, and have been related to the extensional properties of the fluid [7]. Recently, qualitatively similar behavior has been observed in entry flows of low-viscosity elastic fluids in microchannels [27,28] using streak imaging methods; however, velocity fields were not reported.

We characterize the distortion quantitatively at each strain rate by computing the root-mean-square deviation of the velocity field from the Newtonian case at the same $\dot{\epsilon}$ and using this quantity as an order parameter. The velocity fields are first normalized by their respective average magnitudes: $\tilde{\vec{V}} = \vec{V}(x, y) / \langle |\vec{V}(x, y)| \rangle$. We then compute the rms difference $\Delta \tilde{V}_{rms} = \langle |\tilde{\vec{V}}_P - \tilde{\vec{V}}_N|^2 \rangle^{0.5}$, where $\tilde{\vec{V}}_P$ and $\tilde{\vec{V}}_N$ are the polymer and Newtonian velocity fields, respectively. We plot the values of $\Delta \tilde{V}_{rms}$ as a function of $\dot{\epsilon}$ and De in Fig. 3(d). The difference is close to 0 for low $\dot{\epsilon}$, where the velocity fields are nearly identical to their Newtonian counterparts. As $\dot{\epsilon}$ is increased, we compare the growth of $\Delta \tilde{V}_{rms}$ to the square root behavior that is typical of forward bifurcations. The fit is reasonable even above $\dot{\epsilon} = 1.0$ s⁻¹ (De = 12.5), where the flow is time dependent. We do not find significant hysteresis in Fig. 3(d). We find a critical strain rate for the onset of the asymmetric instability and bistability at $\dot{\epsilon} = 0.15$ s⁻¹ (De = 1.8).

We have also done experiments on a dilute solution of a semirigid polymer (xanthan gum, 200 ppm) at the same viscosity and rms shear rate. This solution shows no instability; the velocity field is found to be similar to the Newtonian case.

Although Poiseuille flows of viscoelastic fluids are linearly stable (due to the lack of curved streamlines), the elastic instability near the hyperbolic point of the microchannel strongly perturbs the downstream Poiseuille flow. We demonstrate this fact by plotting in Fig. 4(a) the normalized speed as a function of the transverse channel coordinate, 4 channel widths downstream from the hyperbolic point. The velocity profile for a Newtonian fluid shows the familiar parabolic profile. This is also the case for a PAA solution at $\dot{\epsilon} = 0.1$ s⁻¹ (De = 1.2) (below the instability threshold). However, at higher $\dot{\epsilon} > 1.0$ s⁻¹, e.g., at $\dot{\epsilon} = 1.5$ s⁻¹ (De = 18.6), we find that the velocity profile is asymmetric and time dependent even far downstream.

Achieving efficient mixing in microchannels is not a trivial task because the flow is inherently laminar (Re < 1) due to small length scales. Several methods have been proposed based on temporal or spatial, forcing of the flow, three dimensions, and curved geometries in

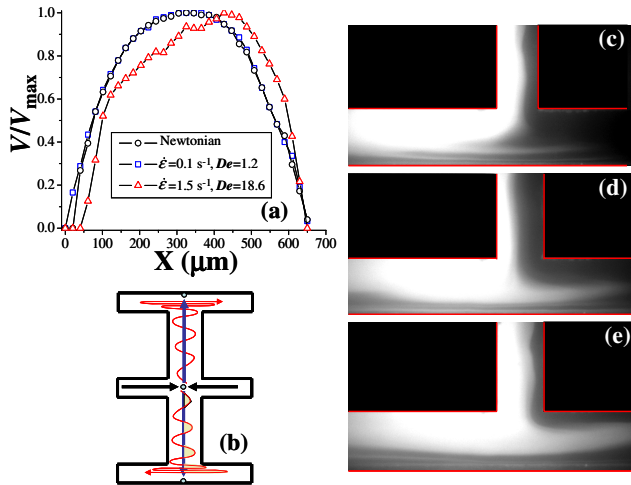


FIG. 4 (color online). (a) Longitudinal velocity (normalized by the maximum value) as a function of the cross-channel coordinate at 4 channel widths downstream of the hyperbolic point, showing the strong distortion caused by the symmetry-breaking instability. (b) Modified apparatus with an extra T at each outlet to promote mixing. (c)–(e) Dye snapshots showing the stretching and folding of fluid elements in one of the end regions that results from the time-dependent instability, at $\dot{\epsilon} = 2.13 \text{ s}^{-1}$ ($De = 26.4$).

conjunction with dilute polymer solutions. (For a review, see [29].) The instabilities documented here can also promote mixing in a simple steadily forced flow. By inserting an extra “ T ” as shown in Fig. 4(b), we find that the extensional flow instabilities cause stretching and folding of fluid elements in the outlet region. This is demonstrated in Figs. 4(c)–4(e), where we show snapshots taken 0.5 s apart. Here, the instability in the cross slot leads to distorted regions of dyed and undyed fluid that are transported to the extra T at the end, where they are stretched and folded as illustrated schematically in Fig. 4(b).

In conclusion, we find that flexible polymer solutions show two distinct instabilities in an extensional cross-channel flow at low $Re (< 10^{-2})$. The first at $\dot{\epsilon} = 0.15 \text{ s}^{-1}$ ($De = 1.8$) leads to spatial symmetry breaking and bistability, while the second at $\dot{\epsilon} = 1.0 \text{ s}^{-1}$ ($De = 12.5$) produces broadband temporal fluctuations. The instabilities were not found for the semirigid polymer solution under comparable conditions. We hypothesize that these instabilities may be controlled by the stretching of polymer molecules near the hyperbolic point. Numerical simulations [13,15], birefringence measurements [20,21], and direct measurements of DNA molecules [12,24] have shown molecular extension in a cross-channel flow above a critical strain rate. Whether the observed flow instabilities in the present are related to the stretch-coil transition found for flexible polymer solutions remains to be determined in subsequent work. Given the clear evidence presented here

that the initial instability is a forward bifurcation, it should be possible to obtain insight into its origin by analysis or computation.

We appreciate helpful conversations with G. Leal, A. Morozov, and W. van Saarloos. This work was supported primarily by NSF DMR-0405187, with additional support by NSF DMR05-20020.

- [1] R.H. Thomas and K. Walters, *J. Fluid Mech.* **18**, 33 (1964).
- [2] A.B. Metzner and J.L. White, *AIChE J.* **11**, 989 (1965).
- [3] H. Giesekus, *Rheol. Acta* **5**, 239 (1966).
- [4] D.V. Boger, *Annu. Rev. Fluid Mech.* **19**, 157 (1987).
- [5] G.H. McKinley *et al.*, *J. Fluid Mech.* **223**, 411 (1991).
- [6] E.S.G. Shaqfeh, *Annu. Rev. Fluid Mech.* **28**, 129 (1996).
- [7] J.P. Rothstein and G.H. McKinley, *J. Non-Newtonian Fluid Mech.* **98**, 33 (2001).
- [8] R.G. Larson, E.S.G. Shaqfeh, and S.J. Muller, *J. Fluid Mech.* **218**, 573 (1990).
- [9] A. Groisman and V. Steinberg, *Nature (London)* **405**, 53 (2000).
- [10] A. Groisman and V. Steinberg, *Nature (London)* **410**, 905 (2001); T. Burghelca *et al.*, *Phys. Rev. E* **69**, 066305 (2004).
- [11] D.E. Smith, H.P. Babcock, and S. Chu, *Science* **283**, 1724 (1999).
- [12] T.T. Perkins, D.E. Smith, and S. Chu, *Science* **276**, 2016 (1997).
- [13] T. Hofmann, R.G. Winkler, and P. Reineker, *Phys. Rev. E* **61**, 2840 (2000).
- [14] G.H. McKinley and T. Sridhar, *Annu. Rev. Fluid Mech.* **34**, 375 (2002).
- [15] C.-C. Hsieh, S.J. Park, and R.G. Larson, *Macromolecules* **38**, 1456 (2005).
- [16] P.G. De Gennes, *J. Chem. Phys.* **60**, 5030 (1974).
- [17] E.J. Hinch, *Colloques Internationaux du C.N.R.S* **233**, 241 (1974).
- [18] R.G. Larson and J.J. Magda, *Macromolecules* **22**, 3004 (1989).
- [19] D.P. Pope and A. Keller, *Colloid Polym. Sci.* **256**, 751 (1978).
- [20] G.G. Fuller and G. Leal, *Rheol. Acta* **19**, 580 (1980).
- [21] A. Keller and J.A. Odell, *Colloid Polym. Sci.* **263**, 181 (1985).
- [22] T.Q. Nguyen, G. Yu, and H.-H. Kausch, *Macromolecules* **28**, 4851 (1995).
- [23] D.E. Smith and S. Chu, *Science* **281**, 1335 (1998).
- [24] C.M. Schroeder *et al.*, *Science* **301**, 1515 (2003).
- [25] D.V. Boger, *J. Non-Newtonian Fluid Mech.* **3**, 87 (1977).
- [26] R.B. Bird *et al.*, *Dynamics of Polymeric Liquids: Fluid Mechanics* (John Wiley & Sons, New York, 1987), Vol. 1.
- [27] A. Groisman, M. Enzelberger, and S.R. Quake, *Science* **300**, 955 (2003).
- [28] L.E. Rodd *et al.*, *J. Non-Newtonian Fluid Mech.* **129**, 1 (2005).
- [29] N.T. Nguyen and Z. Wu, *J. Micromech. Microeng.* **15**, R1 (2005).